HHS Public Access

Author manuscript

Med Devices Sens. Author manuscript; available in PMC 2022 June 27.

Published in final edited form as:

Med Devices Sens. 2021 February ; 4(1): . doi:10.1002/mds3.10139.

A comparative study on silicon nitride, titanium and polyether ether ketone on mouse pre-osteoblast cells

Neelam Ahuja[1], **Kamal R. Awad**[1,2], **Marco Brotto**[1], **Pranesh B Aswath**[2], **Venu Varanasi**[1,2]

[1]Bone-Muscle Research Center, College of Nursing and Health Innovation, University of Texas at Arlington, Arlington, TX, USA

[2]Department of Materials Science and Engineering, University of Texas at Arlington, Arlington, TX, USA

Abstract

The current study provides more insights about the surface bioactivity of the silicon nitride (Si_3N_4) as a potential candidate for bone regeneration in craniofacial and orthopaedic applications compared with conventional implantation materials. Current skeletal reconstructive materials such as titanium and polyether ether ketone (PEEK) are limited by poor long-term stability, biocompatibility and prolonged healing. Si_3N_4 is an FDA-approved material for an intervertebral spacer in spinal fusion applications. It is biocompatible and has antimicrobial properties. Here, we hypothesize that Si_3N_4 was found to be an osteoconductive material and conducts the growth, differentiation of MC3T3-E1 cells for extracellular matrix deposition, mineralization and eventual bone regeneration for craniofacial and orthopaedic applications. MC3T3-E1 cells were used to study the osteoblastic differentiation and mineralization on sterile samples of Si_3N_4, titanium alloy and PEEK. The samples were then analysed for extracellular matrix deposition and mineralization by FTIR, Raman spectroscopy, SEM, EDX, Alizarin Red, qRT-PCR and ELISA. The in vitro study indicates the formation of collagen fibres and mineral deposition on all three sample surfaces. There was more profound and faster ECM deposition and mineralization on Si_3N_4 surface as compared to titanium and PEEK. The FTIR and Raman spectroscopy show formation of collagen and mineral deposition at 30 days for Si_3N_4 and titanium and not PEEK. The peaks shown by Raman for Si_3N_4 resemble closely to natural bone. Results also indicate the upregulation of osteogenic transcription factors such as RUNX2, SP7, collagen type I and osteocalcin. The authors concluded that Si_3N_4 rapidly conducts mineralized tissue formation via extracellular matrix deposition and biomarker expression in mouse calvarial pre-osteoblast cells. Thus, this study confirms that the bioactive Si_3N_4 could be a potential material for craniofacial and orthopaedic applications leading to rapid bone regeneration that resemble the natural bone structure.

Keywords

collagen formation; hydroxyapatite; MC3T3-E1 cells; silicon nitride; titanium

Correspondence: Venu Varanasi, Bone-Muscle Research Center, College of Nursing and Health Innovation, University of Texas at Arlington, TX 76019, USA., venu.varanasi@uta.edu.
Kamal R. Awad and Neelam Ahuja are co-first authors.

1 | INTRODUCTION

Trauma, tumour resection, congenital defects and various medical conditions result in craniomaxillofacial (CMF) and orthopaedic bone defects, which affect either the bony contour or continuity, or both ("Bone Grafts & Substitutes Market by Product (Allografts, Bone Grafts Substitutes, and Cell-based Matrices), by Application (Spinal Fusion, Long Bone, Foot & Ankle, Craniomaxillofacial, Joint Reconstruction, and Dental Bone Grafting)," 2015–2023; *Craniomaxillofacial Implants Market by Product(*Mid Face Implants,Cranial or Neuro Implants,Man-dibular Orthognathic Implants,Distraction Systems,Bone Graft Substitutes,Thoracic Fixation Systems,Total TMJ Replacement Systems,Dural Repair Product, 2017–2023; Neovius & Engstrand, 2010). Although autografts are the gold standard for healing small bone defects, they have limitations in larger defects due to limited bone volume availability at donor site, resorption of the graft, donor site morbidity, chances of infection at both the recipient and donor sites, increased surgical time, patient discomfort and prolonged hospital stay (Kwarcinski et al., 2017; Rogers & Greene, 2012; Zanotti et al., 2016). Further, allografts and xenografts have potential infectious and immunological risks (Hardy & Resident, 2008; "Bone Grafts & Substitutes Market by Product (Allografts, Bone Grafts Substitutes, and Cell-based Matrices), by Application (Spinal Fusion, Long Bone, Foot & Ankle, Craniomaxillofacial, Joint Reconstruction, and Dental Bone Grafting)," 2015–2023; Chiarello et al., 2013). Various alloplastic materials have been developed and are in clinical use for bone replacement procedures (Kwarcinski et al., 2017; Neovius & Engstrand, 2010; Zanotti et al., 2016). A useful reconstructive material/ fixative plate should have the ability to induce new bone formation while stabilizing the defect site without any growth of fibrous tissue at the bone/plate interface (osseointegration) (Albrektsson & Johansson, 2001). Lastly, the reconstructive material should have a sufficient mechanical stability to withstand the implantation procedure and resist the collapse during the patient's normal activities (Thrivikraman et al., 2017).

In our previous study, we compared the use of three basic types of fixative implant/ reconstructive material (polyether ether ketones (PEEK), titanium (Ti6Al4V) and silicon nitride (Si_3N_4)) on their suitability to facilitate surface formation of Ca-P aggregates. Our goal in the prior work was to determine whether a ceramic silicon nitride could produce possible non-cellular-driven mineral formation to assess the potential to form a direct bond with Ca-P aggregates in a similar role as that of Ti-fixative plates. We found that such an effect was comparable with titanium and slightly elevated the potential (in vitro) growth of such aggregates on PEEK (Awad, et al., 2019).

In the present study, we hypothesize that silicon nitride could be an osteoconductive material and enhance growth, differentiation, extracellular matrix (ECM) and mineral deposition of the murine calvarial MC3T3-E1 pre-osteoblast cells. The authors tested this hypothesis by conducting a comparative study of the cellular response to the three surfaces: Ti6Al4V, Si_3N_4 and PEEK. In vitro cell culture studies were performed on the samples surface for 30 and 60 days using MC3T3-E1 cell line. At each time points, samples were collected and used to study the osteoblastic differentiation and mineralization on the sterile samples. The

samples were then analysed for extracellular matrix deposition and mineralization by FTIR, Raman spectroscopy, SEM, EDX and Alizarin Red stain. For qRT-PCR and ELISA, the cells were grown, seeded and differentiated using previously established protocol for 1, 3, 7 and 14 days. Then, qRT-PCR and ELISA studies were performed following our previously published protocol. The results were analysed in a comparative way to cleary compare the surface activity of the Si_3N_4 with Ti6Al4V and PEEK as presented below.

2 | MATERIALS AND METHODS

2.1 | Sample preparation

Samples of silicon nitride were provided and processed by Amedica Corporation with physical properties as given previously (McEntire et al., 2016; Pezzotti et al., 2016). Disc of Ø12.7 × 2.5 mm was prepared for further characterization and in vitro testing. PEEK (ASTM D6262, Ketron® PEEK 1000, Quadrant EPP USA, Inc.; distributed by McMaster-Carr) and titanium alloy (ASTM F136, Ti6Al4V-ELI, distributed by Vincent Metals) samples with the same diameter (Ø12.7 × 2.5 mm) were used for comparison. The samples were immersed in 100% ethanol and ultrasonicated for 5 min to remove any possible surface debris. Sterilization was achieved as previously described (Awad, et al., 2019) using gas sterilization with ethylene oxide for 12 h, and then, vacuum desiccation was performed for 24 h to remove any residual absorbed ethylene oxide gas. Surface cleaning and sterilization were conducted at standard temperature and pressure (i.e. 25°C and 1 bar).

2.2 | In vitro studies

In vitro cell study using murine calvarial MC3T3-E1 pre-osteoblast cells was accomplished to investigate cell differentiation and mineralization on each surface. The experimental studies were conducted at the Bone and Muscle Research Center and Department of Material Science and Engineering at University of Texas at Arlington. All characterizations were carried out at the Center for Characterization of Materials and Biology at the University of Texas at Arlington (CCMB, UTA).

Murine calvarial MC3T3-E1 pre-osteoblast cells (American Type Cell Culture Inc., Manassas, VA) were cultured using α-MEM supplemented with 10% foetal bovine serum (FBS) and 1% penicillin/streptomycin (pen-strep) until 75–90% confluence in 75 sq. cm flasks (Corning Life Sciences Inc.). These cells were used between passages 21 and 29 and incubated at 37°C, 100% relative humidity and 5% CO_2 (according to the manufacturer's specifications). Ethylene oxide-sterilized samples of each test material ($n = 3$) were washed twice with PBS, placed in 24 vacuum gas-treated standard tissue culture well plates (Corning Life Sciences Inc.) and seeded with 10^5 MC3T3-E1 cells for 24 h. To study the osteoblastic differentiation and mineralization on the surface of the samples, the culture medium was replaced with differentiation medium after 24 h of seeding, which consists of α-MEM supplemented with 10% FBS, and 1% pen-strep enriched with 50 μg/ml ascorbic acid (Sigma-Aldrich). The differentiating media were changed every 2 days, and cells were cultured on the surface for 30 days to study ECM deposition and 60 days to study the mineralization. After 30 and 60 days, the samples were washed in PBS twice to remove non-adherent cells and transferred to fresh well plates. The samples were fixed using 2%

glutaraldehyde (Sigma Inc.) for 1 h. The samples were then sequentially alcohol-dehydrated using an ethanol–water mixture using sequential concentrations of alcohol (i.e. 25%, 50%, 75% and 100%) to preserve the intact cellular structure on the sample surfaces. The samples were then analysed using FTIR, SEM and Raman Spectroscopy and then stained with Alizarin Red.

2.3 | FTIR and Raman spectroscopy

FTIR and Raman spectroscopy were conducted on all samples cultured for 30 and 60 days to characterize the ECM formation and mineralization on the different surfaces. FTIR analysis was performed using Thermo Nicolet 6700 FTIR Spectrometer (Thermo Electron Corporation) with a smart attenuated total reflectance (ATR) accessory. The FTIR absorbance spectra were collected over the range of 4000–500 cm^{-1}, with an aperture of 150, 128 scans and resolution of 4 cm^{-1}. Raman spectroscopy (DXR, Thermo Scientific) was conducted for Si_3N_4 and Ti6Al4V samples with a 780 nm excitation laser at 100 mW, 10× objective and a 50 μm slit, whereas for PEEK, Raman spectroscopy was conducted using same excitation laser at 1 mW, 10× objective and a 25 μm pinhole. Photobleaching for 4 minutes was used prior to spectra collection with a 10-s exposure time. Thirty-two spectra per location were recorded between 400 and 2000 cm^{-1}. Raman data from the surfaces of all samples after 60 days of the in vitro study revealed the ECM and mineralization composition. ECM composition can be revealed by the amide peaks and proline of collagen, the mineral content can be indicated by the presence of PO_4^{3-} symmetric stretching vibrational modes (phosphate group of HA), and the Raman intensity is proportional to the mineralization content.

2.4 | HR-SEM and EDS analysis

High-resolution scanning electron microscopy (HR-SEM) was used along with energy-dispersive X-ray spectroscope (EDS) mapping to study the surface morphology of the ECM deposition and mineralization on Si_3N_4 and other samples. All samples were coated with silver using a sputter coater (CrC-100 sputter, Plasma Sciences Inc.) for imaging using an Ultra HR-SEM (Hitachi S-4800 II FE SEM, Hitachi). Working distance of 10 mm under 20 kV was used, and images were taken at different magnifications. EDS mapping of sample surfaces was observed with an EDS detector connected with a Hitachi S-3000N Variable Pressure SEM.

2.5 | Alizarin Red staining

Alizarin Red S staining was performed on the sample surface after 60 days of cell culture to detect calcium by forming Alizarin Red S–calcium complex by chelation. 2% Alizarin Red solution (neutralized by 10% acetic acid and 10% ammonium hydroxide to pH 4.1–4.3) was used to stain all samples for 15–30 minutes to be observed under the microscope for red-orange staining of calcium. The samples were washed to remove excess dye and dehydrated using acetone, and images were conducted using a digital microscope (VHX-6000, Keyence).

2.6 | qRT-PCR analysis

Quantitative reverse transcriptase–polymerase chain reaction (qRT-PCR) was used to study the gene expression of the MC3T3-E1 cells as previously described (Varanasi et al., 2009) on the surface of silicon nitride as compared to PEEK and titanium alloy. The cells were grown, seeded and differentiated using the previously established protocol above for 1, 3, 7 and 14 days. Culture media were collected at each time point and stored at −80°C for further evaluation. qRT-PCR was performed on all samples after days 1,3 and 7 using previously established protocol (Varanasi et al., 2009). Following cell lysing, mRNA was extracted (RNeasy Mini Kit, Qiagen) and reverse-transcribed to cDNA (reverse transcription System, Promega) based on the manufacturer's guidelines. Samples were tested for relative expression of runt-related transcription factor 2 (RUNX2, accession no. NM_009820.2), transcription factor SP7 (SP7, accession no. AF184902.1), collagen type I, alpha 2 (Col1a2, accession no. NM_007743.2) and bone gamma carboxyglutamate protein (BGLAP, accession no. NM_007541.3) using glyceraldehyde 3-phosphate dehydrogenase (GAPDH, accession no. NM_008084.2) as the internal housekeeping gene. Quantification of the relative gene expression was performed with delta−delta CT (Δ−Δ-CT) method.

2.7 | ELISA

The cell culture media were collected at 1, 3, 7 and 14 days to evaluate the protein expression of different samples. The concentration of osteocalcin was determined using an enzyme-linked immunosorbent assay (ELISA) kit (ELISA, Alfa Aesar) per manufacturer guidelines and previously described procedures (Varanasi et al., 2009). Samples were thawed and pipetted into the well plate along with kit standards. The plate was incubated and washed several times. Stop solution was added, and the optical density was measured using a spectrophotometer at 450 nm.

2.8 | Statistical analysis

Statistical analysis was performed with SPSS (IBM Corporation) and Microsoft Excel (Microsoft Corporation), and all data are represented as mean ± *SD*. Mean "average" is an important measure that incorporates the score from every participant in the research study, while the standard deviation is one of the most used statistical measures to demonstrate data variability. Thus, mean and standard deviation are best used when data are normally and symmetrically distributed (Rodrigues et al., 2017). Paired *t* test and one-way analysis of variance with post hoc Tukey's test (between-group comparisons) were used, and the *p* value was set to 0.05. * represents $p < 0.05$, ** represents $p < 0.01$, and ***represents $p < 0.001$.

3 | RESULTS

3.1 | FTIR and Raman spectroscopy

To identify the organic and inorganic components of the ECM environment on the surface of each sample, FTIR analysis within 600–2000 cm^{-1} spectral range was performed. Figure 1a–c represents the FTIR spectra of the samples seeded with MC3T3-E1 cells and cultured in differentiation media for 30 days. Both Si_3N_4 and Ti6Al4V samples exhibited peaks indicating the presence of collagen fibres and mineralization, while the PEEK sample did

not exhibit any significant peaks for the ECM environment. The spectra indicated several vibrational bands related to the ECM components such as ECM proteins (collagen) and P-O bonds of PO_4^{3-} mineral ions on Si_3N_4 and Ti6Al4V surfaces. The presence of ECM proteins on Si_3N_4 and Ti6Al4V surfaces is indicated by the presence of vibrational bands of amide I (peak a at 1637 cm^{-1}), amide II (peak b at 1532 cm^{-1}) and amide III (peak c at 1228 cm^{-1}). The stretching P-O bond (peak d) of PO_4^{3-} at 1030 cm^{-1} confirmed the mineral formation of "inorganic components of the ECM" on Si_3N_4 and Ti6Al4V surfaces, and the presence of a single broad peak spanning by 900–1200 cm^{-1}, which indicated the formation of amorphous calcium phosphate (ACP; Davies et al., 2017). After 60 days of in vitro cell culture, the FTIR spectra revealed the presence of amides I, II and III and the vibrational bands for P-O bond of PO_4^{3-} ions on the surface of all samples (Si_3N_4, Ti6Al4V, and PEEK), indicated in Figure 1d–f.

To gain more details about the composition of ECM and mineral formation on the samples after 60 days of the in vitro cell culture study, Raman analyses were conducted on the three different samples compared with the glass coverslip (GCS) as a control. Figure 2 shows the Raman spectra on the surface of each sample compared with the bare surface and GCS. After analysing the Raman spectra for Si_3N_4, it is clear that Si_3N_4 surface displays peaks for amide I (1665 cm^{-1}), amide III (1255–1272 cm^{-1}) of collagen and the four vibrational modes of phosphate group (symmetric stretching vibration of PO_4^{3-} of HA) at v_1:962 cm^{-1}, v_2:428 cm^{-1}, v_3:1044 cm^{-1} and v_4:589 cm^{-1}. Additional functional groups indicated by peaks included a carbonate peak at 1033 cm^{-1}, collagen proline (853 cm^{-1}) and hydroxyproline at 872 cm^{-1}, as well as CH_2 deformation of proteins at 1446 cm^{-1}. Spectra results for Ti6Al4V samples only confirmed the presence of amide I and amide III of collagen, v_1 and v_3 modes of phosphate and the CH_2 deformation peak. The GCS control only displayed peaks for amide II, v_4 – PO_4^{3-} and CH_2 deformation peak, and PEEK only showed the amide II peak as indicated in Figure 2.

3.2 | HR-SEM and EDS analysis

HR-SEM was used to capture the surface morphology and investigate the formation of collagen fibres and mineral on the different samples. Figure 3 indicates the surface morphology of the samples after 30 days of the in vitro study. From Figure 3a, it should be noted that the Si_3N_4 surface was completely covered with the collagen fibrils that turned into collagen bundles as indicated by the arrows. Furthermore, mineral (ACP) deposition was observed on the surface using high magnification imaging and confirmed the FTIR and Raman results. HR-SEM images also confirmed the presence of collagen fibres and mineral deposition on the surface of Ti6Al4V samples (Figure 3b). Although the high magnification images indicated that collagen fibres started to form collagen bundles on Ti6Al4V, the surface was not completely covered by the collagen fibres. Also, sparse deposition of ACP was detected on the surface of Ti6Al4V samples. On the other hand, SEM images of the PEEK samples revealed the presence of collagen fibrils, but no collagen bundles were detected. Moreover, the PEEK surface was not completely covered by collagen fibres. The poor ECM formations on the PEEK surfaces could be attributed to the low number of

attached cells leading to low differentiation and poor ECM deposition. Figure 4 presents the HR-SEM images at different magnifications for all samples to investigate the ECM mineralization after 60 days of the in vitro study. A “flower-like” porous ACP structure was deposited on Si_3N_4 and Ti6Al4V samples, covering the surfaces. Although mineral deposition on Ti6Al4V surfaces covered a comparable area to Si_3N_4 deposition, the later still has the highest coverage area as indicated in Figure 3a. After 60 days, PEEK sample surfaces were covered with collagen bundles, while ACP deposition was sparse.

The energy-dispersive X-ray spectroscopy (EDS) mapping was used to determine the surface morphology, composition and element distribution of the mineral deposition. Regions of interest corresponding to ACP deposition were defined by mapping the surfaces and detecting the Ca and P K edges. After 30 days of the in vitro study, only Ca and P deposition was observed on the surface of Si_3N_4 samples as shown in Figure 5a. This could be attributed to the high density of mineral deposition on the surface of Si_3N_4 compared with Ti6Al4V and PEEK samples. Figure 5b–d presents the EDS mapping of the samples after 60 days which clearly identified the presence of mineral deposition on the surface of all samples, with high-density deposition of Ca and P deposition on Si_3N_4 surfaces (Figure 5b).

3.3 | Alizarin Red staining

Alizarin Red S staining confirmed calcium deposition on the sample surfaces. Similar to the SEM results, a deep red-orange stain was observed on Si_3N_4 and Ti6Al4V indicating extracellular calcium deposition, shown in Figure 6. Calcium deposition was observed on PEEK surfaces but with less intensity.

3.4 | qRT-PCR and ELISA

qRT-PCR results indicated significantly higher relative expression of collagen I on day 1 and day 3 of differentiation for titanium alloy and silicon nitride, shown in Figure 7a. There was an almost fourfold increase in collagen I expression in silicon nitride samples compared with glass coverslip after 3 days. RUNX2 expression (Figure 7b) was significantly enhanced for Ti6Al4V at day 1, about threefold greater than RUNX2 expression in GCS samples, but there was no significant difference in the silicon nitride and GCS samples, despite a twofold increase compared with glass coverslip. There was a significant 2.5-fold increase in RUNX2 expression in both Ti6Al4V and Si_3N_4 samples after 3 and 7 days of differentiation compared with PEEK and glass coverslip. Graph 7 (c) shows the expression of Osterix determined (SP7) by qRT-PCR. There was a significant twofold increase in SP7 expression for Ti6Al4V and Si_3N_4 samples as compared to glass coverslip and PEEK. Osteocalcin (OCN) concentration, determined by ELISA, was significantly enhanced after 3 days of differentiation, and relatively increased after 7 days of culture for both Ti6Al4V and Si_3N_4 as shown in graph 7 (d). All gene expression data, and the ECM and mineralization analysis results are summarized as shown in Table 1.

4 | DISCUSSION

Recent studies of silicon nitride have characterized its properties for protein adsorption, antimicrobial and osseointegration (Pezzotti, et al., 2017; Pezzotti, et al., 2017; Webster et

al., 2012). These properties may be useful for orthopaedic and craniofacial applications. In this study, we evaluated the osteoconductive nature of the silicon nitride as opposed to titanium and PEEK. We found evidence of ECM deposition and mineral formation on all three different surfaces, that is Si_3N_4, Ti6Al4V and PEEK after 30 and 60 days of in vitro study. It was noted that the relatively high densities of ECM and minerals were formed on the silicon nitride samples, confirmed by HR-SEM. Also, Si_3N_4 surfaces were completely covered by collagen bundles and ACP particles, while slightly lower ECM coverage and minimal ACP deposition were observed on Ti6Al4V and PEEK surfaces. Bare Ti6Al4V and PEEK surfaces were observed in multiple SEM images. FTIR and Raman spectroscopy supported SEM findings, revealing enhanced mineral deposition and extracellular matrix formation on the surfaces of Si_3N_4 surfaces compared with Ti6Al4V and PEEK.

FTIR analysis revealed the presence of vibrational bands and P-O stretching typically exhibited by ECM proteins based on previously described literature (Davies et al., 2017; Megat Abdul Wahab et al., 2017ahab et al., 2017). A significant single broad peak spanning 900–1200 cm^{-1} (P-O peak) (refers to the formation of amorphous calcium phosphate (ACP; Davies et al., 2017)) was observed, indicating the formation of either calcium phosphate or hydroxyapatite on the surface of Si_3N_4 and Ti6Al4V after just 30 days of in vitro study. It is important to note that the intensity of the P-O peak was relatively higher for Si_3N_4 surfaces compared with Ti6Al4V surfaces as shown in Figure 1a,b indicating increased mineral content on Si_3N_4 surfaces compared with Ti6Al4V surfaces, which is confirmed by SEM findings. On the other hand, PEEK samples did not show any peaks related to ECM environment after 30 days as indicated in Figure 1c. The absence of collagen and/or mineral formation on the PEEK surfaces could be attributed to the low surface energy, hydrophobic nature and surface smoothness, leading to low protein adsorption and less cell attachment, resulting in little to no collagen or mineral deposition (Kurtz & Devine, 2007; Pelletier et al., 2016; Torstrick et al., 2017; Tsougeni et al., 2009). After 60 days of culture, FTIR results indicated the presence of ECM and mineral on all three sample surfaces (Si_3N_4, Ti6Al4V and PEEK) as seen in Figure 1d–f. The intensity of amides and PO_4^{3-} peaks at 60 days increased relative to peak intensity at 30 days for Si_3N_4 and Ti6Al4V surfaces. Additionally, a shift in amide 1 peak position, represented by two closed peaks at 1659 and 1628 cm^{-1}, could be attributed to the presence of collagen/Ca^{2+} structure (Zhang et al., 2003).

Interestingly, significant peaks for ECM and mineral content observed in the Raman spectra for Si_3N_4 surfaces were similar to previously established peaks found in the spectra of actual bone (Buchwald et al., 2012; Draper et al., 2005; Ilyas et al., 2016). The intensity of $v_1 - PO_4^{3-}$ peak accounts for the mineral content, and the full width at half maximum (FWHM) of that peak is proportional to the maturity of the crystals, representing the c-axis length (Ilyas et al., 2016). Thus, it is very important to note that the PO_4^{3-} peak intensity was greater for Si_3N_4 surfaces compared with Ti6Al4V surfaces. Also, FWHM was greater for Si_3N_4 compared with Ti6Al4V, confirming the formation of mature mineral crystals on the Si_3N_4 sample surface. The enhanced ECM and mineral formation on the silicon nitride surface can be attributed to its surface bioactivity and higher surface energy resulting in rapid and dense ECM and HA formation compared with the Ti6Al4V surface as reported. On the other hand, the spectra for PEEK samples only revealed peaks for amide II, and

the spectra for GCS samples displayed peaks for amide II, CH_2 deformation and a broad peak for $v_4 - PO_4^{3-}$, which can be attributed to the bioinertness and hydrophobic properties of these surfaces. The results of FTIR and Raman Spectroscopy suggest increased mineral deposition and dense extracellular matrix formation on Si_3N_4 surfaces, possibly due to enhanced MC3T3-E1 pre-osteoblast cell growth and differentiation.

EDS results confirmed the presence of Ca and P deposition on the surface of each sample that were previously indicated by the SEM images, FTIR and Raman spectroscopy. It is important to note the regions of high Ca and P deposition density compared with the main element's distribution of the sample. For example, on the Si_3N_4 sample, the increased density deposition of Ca and P slightly shield the Si_3N_4 surface, resulting in decreased displayed Si density in these regions.

To visualize the calcium mineral deposition on material surfaces, Alizarin Red staining was performed. SEM results, indicating that ECM and mineral formation are delayed on Ti6Al4V and PEEK surfaces compared with Si_3N_4 due to high-density surface coverage of the ECM on Si_3N_4 surfaces, were confirmed by Alizarin Red staining. Low surface energy and lack of surface functional groups that act as precursors for collagenous ECM formation are likely main reasons for poor ECM deposition on Ti6Al4V and PEEK (Pelletier et al., 2016; Tsou et al., 2015; Tsougeni et al., 2009). On the contrary, increased cell attachment, growth, and proliferation and promotion of collagenous biomineral deposition observed on Si_3N_4 surfaces can be attributed to its hydrophilic nature, high surface energy and presence of Si-O and Si-N surface bonding (Deng et al., 2015; Gorth et al., 2012).

Type 1 collagen is the most abundant extracellular matrix protein in bone and provides structural support, making it important for differentiation and organization of the bony tissues. Increased expression of collagen I induced by silicon nitride signifies osteoblastic induction of collagen synthesis in the extracellular matrix. $\alpha 2\beta 1$ integrin mediator binds the collagenous matrix to the osteogenic cell membrane, which induces the mitogen-activated protein kinases (MAPK; Xiao et al., 2002). These kinases phosphorylate and activate RUNX2 and OSX, bone-specific transcription factors important for bone formation and mineralization (Artigas et al., 2014; Xiao et al., 2002). These transcription factors bind to the promoter regions of certain downstream genes such as osteocalcin, often used as a serum marker to detect osteoblastic activity and bone formation due to its role in osteoblastic maturation and hydroxyapatite nucleation (Xiao et al., 2002; Zoch et al., 2016). Previous studies have shown that osteocalcin acts like a bridge between the bone matrix proteins and mineralization in the process of bone formation (Hauschka & Carr, 1982; Hoang et al., 2003; Ritter et al., 1992).

While the use of porous ceramic materials (i.e. Si_3N_4) in osseointegration applications is beneficial due to unique surface properties, some limitations could be arising due to the use of solid body ceramics for CMF applications. One of the main challenges is the lack of tensile strength to give the fixative plate some flexure when fixated into curved bony structures. Therefore, bulk ceramic or polymeric materials with low tensile strength (i.e. Si_3N_4 ~350–400 MPa, and PEEK ~100–110 MPa) are not optimal for load bearing applications compared with tensile materials such as Ti-alloys (~920–980 MPa; Bal &

Rahaman, 2012). The benefits of Si_3N_4 surfaces relative to Ti6Al4V or PEEK in conjunction with limitations in tensile strength imply that Si_3N_4 may serve as a better coating material as opposed to a full body ceramic implanted into the bone. In this direction, we investigated Si_3N_4 and silicon oxynitride (SiO_xN_y) thin film coatings deposited using low-temperature plasma-enhanced chemical vapour deposition (PECVD) techniques (Ahuja et al., 2020; AWAD et al., 2020; Awad, et al., 2019; Monte et al., 2019). Currently, studies on the use of silicon oxynitride coatings, which have demonstrated superior osteogenic properties compared with the materials studied here, are underway (Ahuja et al., 2020; AWAD et al., 2020; Awad, et al., 2019; Ilyas et al., 2015; Varanasi et al., 2017). Using these coatings, we can bring the unique surface properties of Si_3N_4 and SiO_xN_y to the inert surface of reconstructive fixative materials (e.g. titanium plates). Furthermore, other biologically important elements such as phosphorus can be incorporated in the coatings for optimal biological activity (Monte et al., 2019), potentially aiding in the conduction of new bone on these fixative implant surfaces. Thus, the future research will focus on studying the viability of the amorphous SiONx/SiONPx-PECVD thin films as potential coatings for Ti and bioinert implant materials for enhanced osseointegration and rapid bone regeneration.

5 | CONCLUSION

In the current study, we report that silicon nitride surface has comparable mineralized tissue formation via extracellular matrix deposition and bone biomarker expression, in mouse calvarial preosteoblasts cells, to Ti6Al4V surface activity and superior to PEEK surface activity. The results revealed that there was ECM deposition and mineralization on silicon nitride surfaces. The FTIR, Raman spectroscopy and HR-SEM imaging results indicate formation of collagen and mineral deposition after 30 days on silicon nitride and titanium surfaces, but not PEEK surfaces, and the peaks displayed by the Raman spectra for silicon nitride resemble natural biomineral. Results from qRT-PCR assay and ELISA included the upregulation of osteogenic transcription factors such as RUNX2, SP7, collagen type I and osteocalcin. While these results indicate that there are some advantages to the use of silicon nitride surfaces over Ti6Al4V and PEEK, they are counterbalanced by challenges associated with full body ceramics. We recommend investigation into the crystalline or amorphous form of silicon nitride as a coating for Ti6Al4V or PEEK for possible CMF applications.

ACKNOWLEDGEMENTS

The authors want to acknowledge the NIH/NIDCR for their support (1R56-DE027964-01A1-01), Texas STARs award, Departmental Start-up Funds, University of Texas at Arlington, College of Nursing and Health Innovation, Arlington, TX. The authors want to thank Dr. Bryan J. McEntire and Ryan M. Bock of Amedica Corporation for their assistance in providing samples. We also want to acknowledge all our laboratory members, Henry Tran, Sara Peper, Thy Vo, for their support and helpful suggestions.

REFERENCES

Ahuja N, Awad K, Fiedler M, Aswath P, Brotto M, & Varanasi V (2020). Preliminary study of in-situ 3D bioprinted nano-silicate biopolymer scaffolds for muscle repair in VML defects. The FASEB Journal, 34(S1), 1. 10.1096/fasebj.2020.34.s1.03514

Albrektsson T, & Johansson C (2001). Osteoinduction, osteoconduction and osseointegration. European Spine Journal : Official Publication of the European Spine Society, the European Spinal

Deformity Society, and the European Section of the Cervical Spine Research Society, 10(Suppl 2), S96–S101. 10.1007/s005860100282

Artigas N, Ureña C, Rodríguez-Carballo E, Rosa JL, & Ventura F (2014). Mitogen-activated protein kinase (MAPK)-regulated interactions between Osterix and Runx2 are critical for the transcriptional osteogenic program. The Journal of Biological Chemistry, 289(39), 27105–27117. 10.1074/jbc.M114.576793 [PubMed: 25122769]

Awad KR, Ahuja N, Fiedler M, Huang J, Brotto L, Aswath P, Brotto M, & Varanasi V (2020). Micro-patterned bioactive amorphous silicon oxynitride enhances adhesion, growth, and myotubes and axon alignment in muscle and nerve cells. The FASEB Journal, 34(S1), 1. 10.1096/fasebj.2020.34.s1.02245

Awad KR, Ahuja N, Shah A, Tran H, Aswath PB, Brotto M, & Varanasi V (2019). Silicon nitride enhances osteoprogenitor cell growth and differentiation via increased surface energy and formation of amide and nanocrystalline HA for craniofacial reconstruction. Medical Devices & Sensors, 2(2), e10032. 10.1002/mds3.10032

Awad KR, Huang J, Brotto L, Aswath P, Brotto M, & Varanasi V (2019). Patterned silicon oxynitride (SiONx) scaffolds enhance alignment and myogenic differentiation of C2C12 muscle cells. The FASEB Journal, 33(1_supplement), 539.535. 10.1096/fasebj.2019.33.1_supplement.539.5

Bal BS, & Rahaman MN (2012). Orthopedic applications of silicon nitride ceramics. Acta Biomaterialia, 8(8), 2889–2898. 10.1016/j.actbio.2012.04.031 [PubMed: 22542731]

Bone Grafts and Substitutes Market by Product (Allografts, Bone Grafts Substitutes, and Cell-based Matrices), by Application (Spinal Fusion, Long Bone, Foot & Ankle, Craniomaxillofacial, Joint Reconstruction, and Dental Bone Grafting). (2015–2023). From Global Opportunity Analysis and Industry Forecast. Retrieved from https://www.alliedmarketresearch.com/bone-graft-substitutes-market

Buchwald T, Kozielski M, & Szybowicz M(2012). Determination of collagen fibers arrangement in bone tissue by using transformations of Raman spectra maps. Spectroscopy: an International Journal, 27(2), 11. 10.1155/2012/261487

Chiarello E, Cadossi M, Tedesco G, Capra P, Calamelli C, Shehu A, & Giannini S (2013). Autograft, allograft and bone substitutes in reconstructive orthopedic surgery. Aging Clinical and Experimental Research, 25(1), 101–103. 10.1007/s40520-013-0088-8

Craniomaxillofacial Implants Market by Product (Mid Face Implants, Cranial or Neuro Implants, Mandibular Orthognathic Implants, Distraction Systems, Bone Graft Substitutes, Thoracic Fixation Systems, Total TMJ Replacement Systems, Dural Repair Product. (2017–2023). Retrieved from : www.alliedmarketresearch.comhttps://www.alliedmarketresearch.com/craniomaxillofacial-implants-market

Davies OG, Cox SC, Williams RL, Tsaroucha D, Dorrepaal RM, Lewis MP, & Grover LM (2017). Annexin-enriched osteoblast-derived vesicles act as an extracellular site of mineral nucleation within developing stem cell cultures. Scientific Reports, 7(1), 12639. 10.1038/s41598-017-13027-6 [PubMed: 28974747]

Deng Y, Liu X, Xu A, Wang L, Luo Z, Zheng Y, & Wei S (2015). Effect of surface roughness on osteogenesis in vitro and osseointegration in vivo of carbon fiber-reinforced polyetheretherketone–nanohydroxyapatite composite. International Journal of Nanomedicine, 10, 1425–1447. 10.2147/IJN.S75557 [PubMed: 25733834]

Draper ER, Morris MD, Camacho NP, Matousek P, Towrie M, Parker AW, & Goodship AE (2005). Novel assessment of bone using time-resolved transcutaneous Raman spectroscopy. Journal of Bone and Mineral Research, 20(11), 1968–1972. 10.1359/JBMR.050710 [PubMed: 16234970]

Gorth DJ, Puckett S, Ercan B, Webster TJ, Rahaman M, & Bal BS (2012). Decreased bacteria activity on Si(3)N(4) surfaces compared with PEEK or titanium. International Journal of Nanomedicine, 7, 4829–4840. 10.2147/IJN.S35190 [PubMed: 22973102]

Grove DPM Jason R. (2008). Autograft, Allograft and Xenograft Options in the Treatment of Neglected Achilles Tendon Ruptures: A Historical Review with Illustration of Surgical Repair. The Foot & Ankle Journal, 1, (5). 10.3827/faoj.2008.0105.0001

Hauschka PV, & Carr SA (1982). Calcium-dependent alpha-helical structure in osteocalcin. Biochemistry, 21(10), 2538–2547 [PubMed: 6807342]

Hoang QQ, Sicheri F, Howard AJ, & Yang DS (2003). Bone recognition mechanism of porcine osteocalcin from crystal structure. Nature, 425(6961), 977–980. 10.1038/nature02079 [PubMed: 14586470]

Ilyas A, Lavrik NV, Kim HKW, Aswath PB, & Varanasi VG (2015). Enhanced interfacial adhesion and osteogenesis for rapid “bone-like” biomineralization by PECVD-based silicon oxynitride overlays. ACS Applied Materials & Interfaces, 7(28), 15368–15379. 10.1021/acsami.5b03319 [PubMed: 26095187]

Ilyas A, Odatsu T, Shah A, Monte F, Kim HKW, Kramer P, Aswath PB, & Varanasi VG (2016). Amorphous silica: A new antioxidant role for rapid critical-sized bone defect healing. Advanced Healthcare Materials, 5(17), 2199–2213. [PubMed: 27385056]

Kurtz S, & Devine J (2007). PEEK biomaterials in trauma, orthopedic, and spinal implants. Biomaterials, 28(32), 4845–4869. [PubMed: 17686513]

Kwarcinski Jeremy, Boughton Philip, Ruys Andrew, Doolan Alessandra, van Gelder James (2017). Cranioplasty and Craniofacial Reconstruction: A Review of Implant Material, Manufacturing Method and Infection Risk. Applied Sciences, 7(3), 276. 10.3390/app7030276

McEntire Bryan J, Lakshminarayanan Ramaswamy, Thirugnanasambandam Prabhakar, Sampson Jacob Seitz, Bock Ryan, Brien David O (2016). Processing and Characterization of Silicon Nitride Bioceramics. Bioceramics Development and Applications, 06(01). 10.4172/2090-5025.1000093

Megat Abdul Wahab R, Mohamed Rozali NA, Senafi S, Zainol Abidin IZ, Zainal Ariffin Z, & Zainal Ariffin SH (2017). Impact of isolation method on doubling time and the quality of chondrocyte and osteoblast differentiated from murine dental pulp stem cells. PeerJ, 5, e3180. 10.7717/peerj.3180 [PubMed: 28626603]

Monte F, Awad KR, Ahuja N, Kim H, Aswath P, Brotto M, & Varanasi VG (2019). Amorphous silicon oxynitrophosphide coated implants boost angiogenic activity of endothelial cells. Tissue Engineering Part A, 26, 15–27. 10.1089/ten.TEA.2019.0051 [PubMed: 31044666]

Neovius E, & Engstrand T (2010). Craniofacial reconstruction with bone and biomaterials: review over the last 11 years. Journal of Plastic, Reconstructive & Aesthetic Surgery, 63(10), 1615–1623.

Pelletier MH, Cordaro N, Punjabi VM, Waites M, Lau A, & Walsh WR (2016). PEEK versus Ti interbody fusion devices: Resultant fusion, bone apposition, initial and 26-week biomechanics. Clinical Spine Surgery, 29(4), E208–E214. 10.1097/BSD.0b013e31826851a4 [PubMed: 22801456]

Pezzotti G, Bock RM, Adachi T, Rondinella A, Boschetto F, Zhu W, Marin E, McEntire B, Bal BS, & Mazda O (2017). Silicon nitride surface chemistry: A potent regulator of mesenchymal progenitor cell activity in bone formation. Applied Materials Today, 9(Supplement C), 82–95. 10.1016/j.apmt.2017.05.005

Pezzotti G, McEntire BJ, Bock R, Boffelli M, Zhu W, Vitale E, Puppulin L, Adachi T, Yamamoto T, Kanamura N, & Bal BS (2016). Silicon nitride: A synthetic mineral for vertebrate biology. Scientific Reports, 6, 31717. 10.1038/srep31717 [PubMed: 27539146]

Pezzotti G, Oba N, Zhu W, Marin E, Rondinella A, Boschetto F, McEntire B, Yamamoto K, & Bal BS (2017). Human osteoblasts grow transitional Si/N apatite in quickly osteointegrated Si3N4 cervical insert. Acta Biomaterialia, 64(Supplement C), 411–420. 10.1016/j.actbio.2017.09.038 [PubMed: 28963015]

Ritter NM, Farach-Carson MC, & Butler WT (1992). Evidence for the formation of a complex between osteopontin and osteocalcin. Journal of Bone and Mineral Research, 7(8), 877–885. 10.1002/jbmr.5650070804 [PubMed: 1442202]

Rodrigues CFDS, Lima FJCD, & Barbosa FT (2017). Importance of using basic statistics adequately in clinical research. Brazilian Journal of Anesthesiology (English Edition), 67(6), 619–625. 10.1016/j.bjane.2017.01.011

Rogers GFMDJDMBAMPH, & Greene AKMDM (2012). Autogenous bone graft: Basic science and clinical implications. Journal of Craniofacial Surgery, 23(1), 323–327. [PubMed: 22337435]

Thrivikraman G, Athirasala A, Twohig C, Boda SK, & Bertassoni LE (2017). Biomaterials for craniofacial bone regeneration. Dental Clinics of North America, 61(4), 835–856. 10.1016/j.cden.2017.06.003 [PubMed: 28886771]

Torstrick FB, Safranski DL, Burkus JK, Chappuis JL, Lee CSD, Guldberg RE, Gall K, & Smith KE (2017). Getting PEEK to stick to bone: The development of porous PEEK for interbody fusion devices. Techniques in Orthopaedics, 32(3), 158–166. [PubMed: 29225416]

Tsou H-K, Chi M-H, Hung Y-W, Chung C-J, & He J-L (2015). In vivo osseointegration performance of titanium dioxide coating modified polyetheretherketone using Arc ion plating for spinal implant application. BioMed Research International, 2015, 328943. 10.1155/2015/328943 [PubMed: 26504800]

Tsougeni K, Vourdas N, Tserepi A, Gogolides E, & Cardinaud C (2009). Mechanisms of oxygen plasma nanotexturing of organic polymer surfaces: From stable super hydrophilic to super hydrophobic surfaces. Langmuir, 25(19), 11748–11759. 10.1021/la901072z [PubMed: 19788226]

Varanasi V, Ilyas A, Velten M, Shah A, Lanford W, & Aswath P (2017). Role of hydrogen and nitrogen on the surface chemical structure of bioactive amorphous silicon oxynitride films. The Journal of Physical Chemistry B, 121(38), 8991–9005. [PubMed: 28825836]

Varanasi VG, Saiz E, Loomer PM, Ancheta B, Uritani N, Ho SP, Tomsia AP, Marshall SJ, & Marshall GW (2009). Enhanced osteocalcin expression by osteoblast-like cells (MC3T3-E1) exposed to bioactive coating glass (SiO2-CaO-P2O5-MgO-K2ONa2O system) ions. Acta Biomaterialia, 5(9), 3536–3547. 10.1016/j.actbio.2009.05.035 [PubMed: 19497391]

Webster TJ, Patel AA, Rahaman MN, & Sonny Bal B (2012). Anti-infective and osteointegration properties of silicon nitride, poly(ether ether ketone), and titanium implants. Acta Biomaterialia, 8(12), 4447–4454. [PubMed: 22863905]

Xiao G, Gopalakrishnan R, Jiang D, Reith E, Benson MD, & Franceschi RT (2002). Bone morphogenetic proteins, extracellular matrix, and mitogen-activated protein kinase signaling pathways are required for osteoblast-specific gene expression and differentiation in MC3T3-E1 cells. Journal of Bone and Mineral Research, 17(1), 101–110. 10.1359/jbmr.2002.17.1.101 [PubMed: 11771655]

Zanotti B, Zingaretti N, Verlicchi A, Robiony M, Alfieri A, & Parodi P (2016). Cranioplasty: Review of materials. The Journal of Craniofacial Surgery, 27(8), 2061–2072. [PubMed: 28005754]

Zhang W, Huang Z-L, Liao S-S, & Cui F-Z (2003). Nucleation sites of calcium phosphate crystals during collagen mineralization. Journal of the American Ceramic Society, 86(6), 1052–1054. 10.1111/j.1151-2916.2003.tb03422.x

Zoch ML, Clemens TL, & Riddle RC (2016). New insights into the biology of osteocalcin. Bone, 82, 42–49. 10.1016/j.bone.2015.05.046 [PubMed: 26055108]

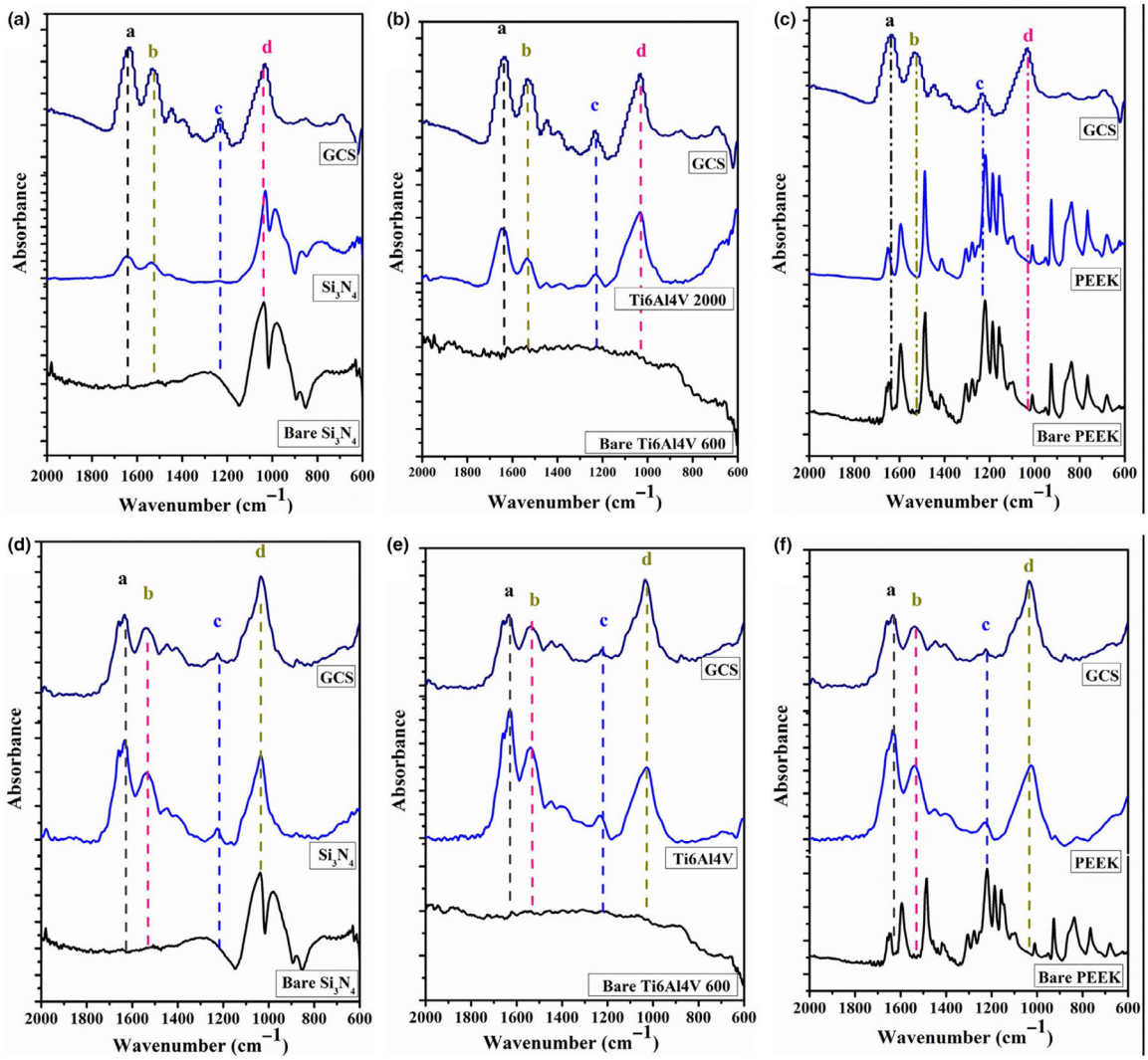

FIGURE 1.

Presents the FT-IR spectra of the of Si3N4, titanium alloy (Ti6Al4V), and PEEK samples showing the matrix deposition of MC3T3-E1 cells cultured in differentiating media for 30 days (a-c) and 60 days (de) of in vitro study. Peaks indicator (a→amide I, b→amide II, c→amide III, and d→P-O bond).

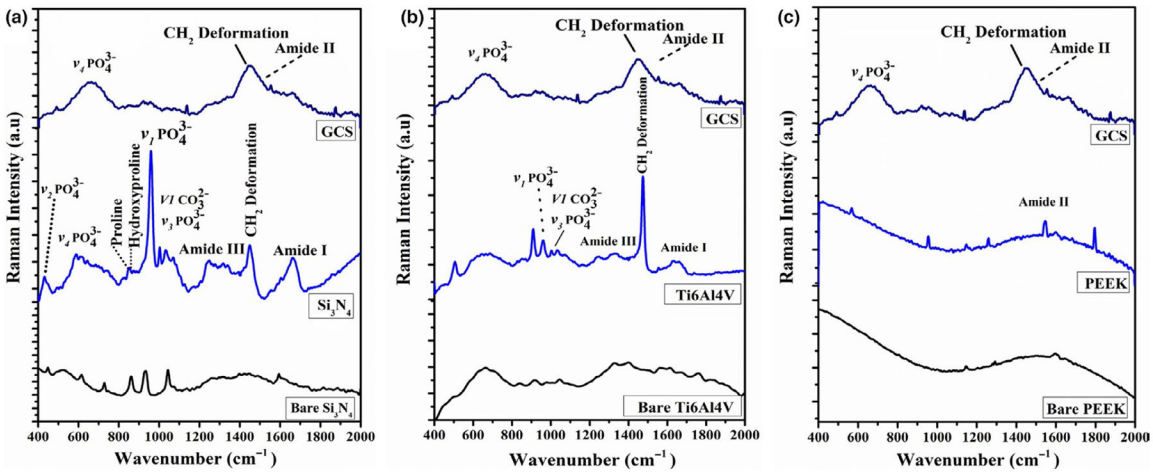

FIGURE 2.

Represents the Raman spectra of Si3N4, titanium alloy (Ti6Al4V), and PEEK samples showing the matrix deposition of MC3T3-E1 cells cultured in differentiating media for 60 days of the in vitro study.

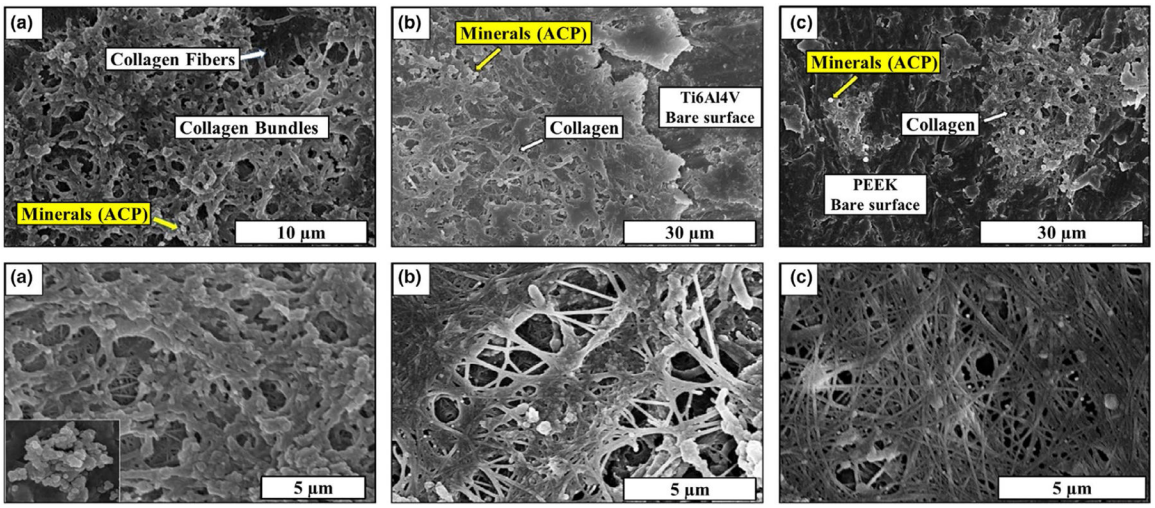

FIGURE 3.

HR-SEM images at different magnification for (a) Si3N4, (b) Ti6Al4V, and c) PEEK samples showing the matrix deposition after 30 days of the in vitro study.

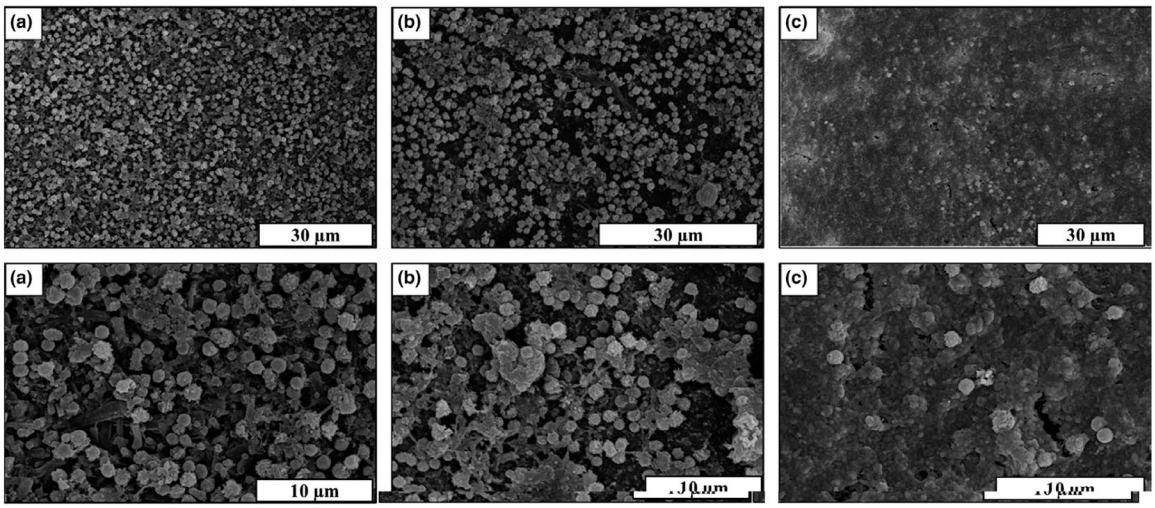

FIGURE 4.

HR-SEM images at different magnification for (a) Si3N4, (b) Ti6Al4V, and (c) PEEK samples showing the matrix deposition after 60 days of the in vitro study.

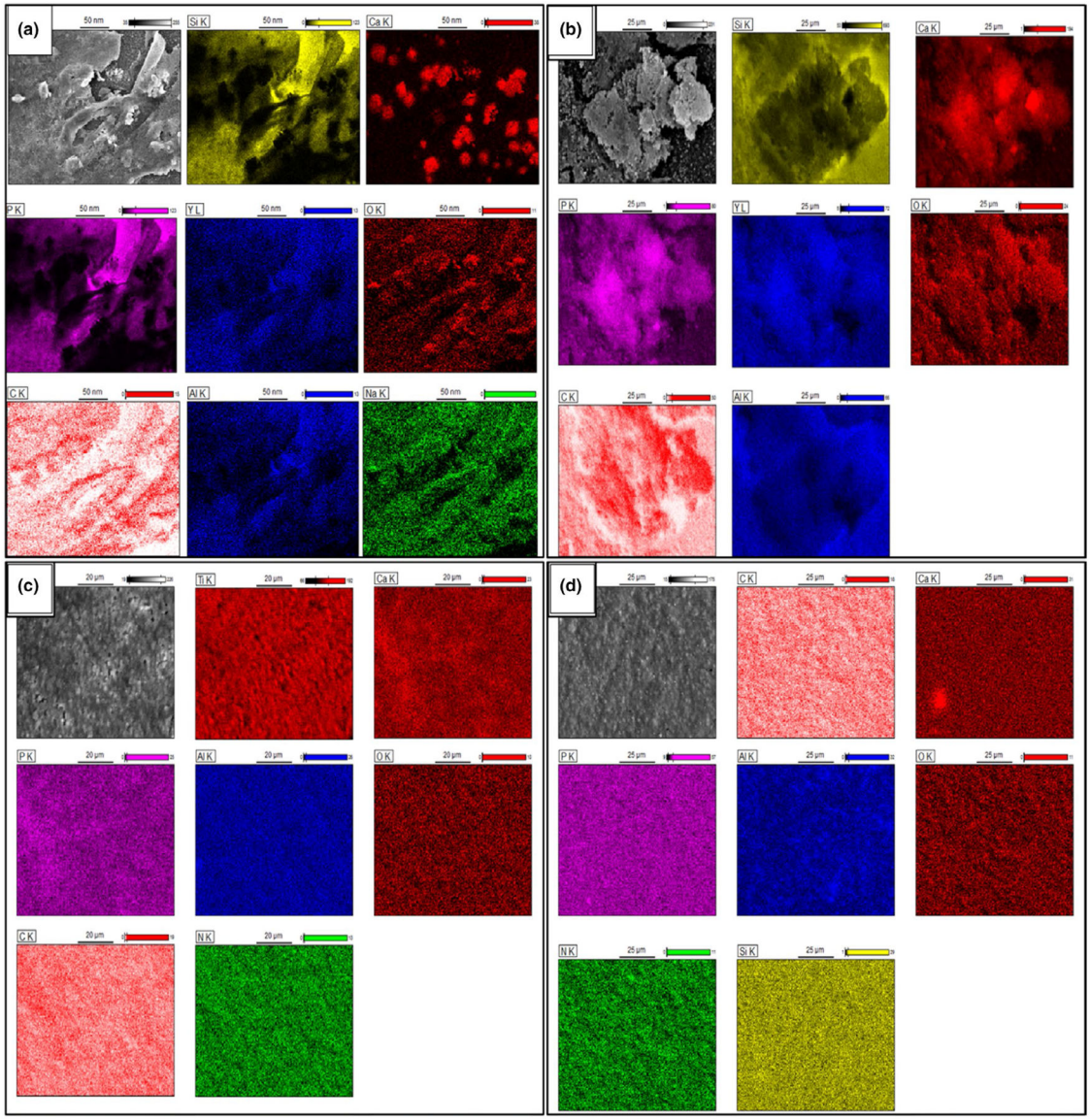

FIGURE 5.

(a) EDS mapping of Si3N4 sample showing the matrix deposition after 30 days of in vitro study, (b-d) EDS mapping of (b) Si3N4, (c) Ti6Al4V, and (d) PEEK sample showing the matrix deposition after 60 days of the in vitro study.

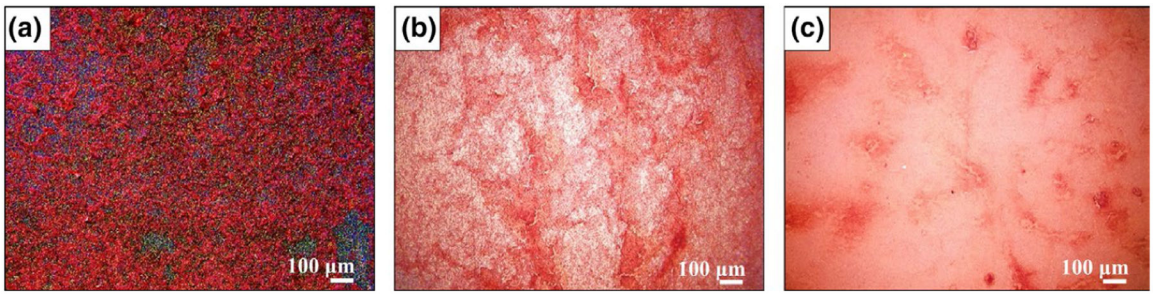

FIGURE 6.

Alizarin red staining for calcium deposition on the surfaces a) Silicon Nitride, b) Titanium alloy, and c) PEEK.

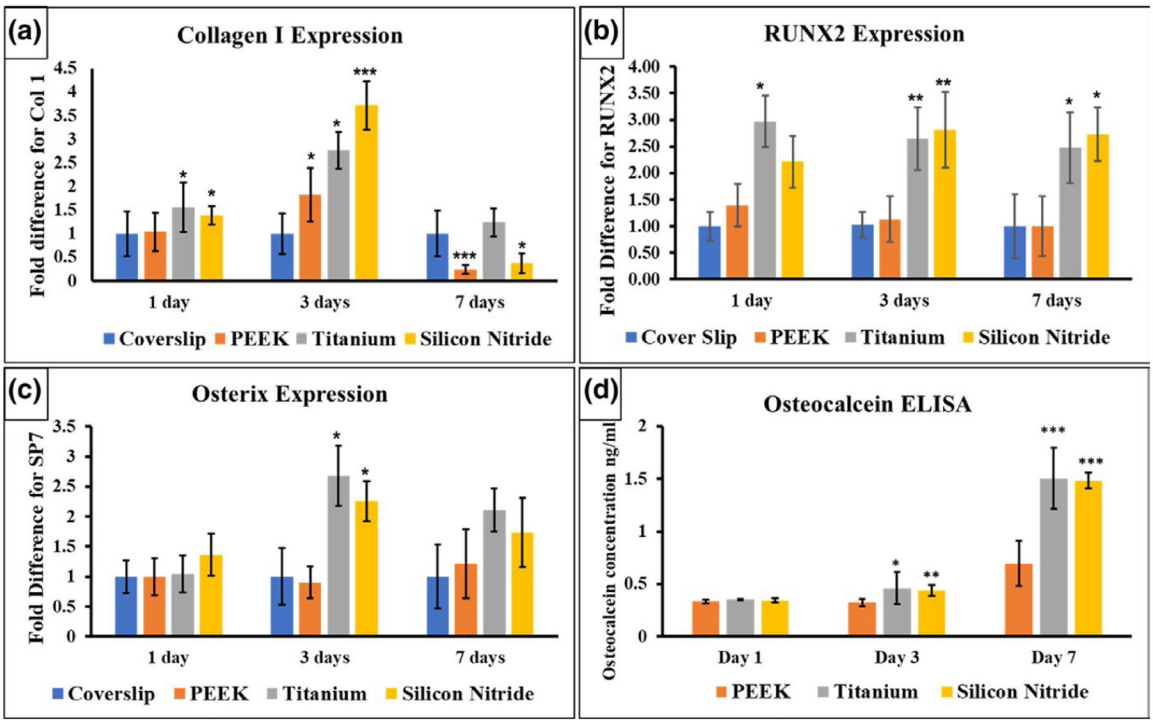

FIGURE 7.

qRT-PCR results show the gene expression of (a) collagen I, (b) RUNX2, and (c) Osterix at 1, 3, and 7 days. (d) Osteocalcin (OCN) measured by ELISA.

TABLE 1

Summary of the ECM, mineralization, *qRT-PCR and ELISA* results on the different surfaces.

Results	Silicon nitride		Ti alloy		PEEK	
ECM and mineralization	**30 Days**	**60 Days**	**30 Days**	**60 Days**	**30 Days**	**60 Days**
Amide I (1,637 cm^{-1}, FTIR)	✓	✓	✓	✓	×	✓
Amide II (1,532 cm^{-1}, FTIR)	✓	✓	✓	✓	×	✓
Amide III (1,228 cm^{-1}, FTIR)	✓	✓	✓	✓	×	✓
P-O @PO_4^{3-} (1,030 cm^{-1}, FTIR)	✓	✓	✓	✓	×	✓
ACP @ (900 – 1,200 cm^{-1}, FTIR)	✓	✓	✓	✓	×	✓
V_1 CO_3^{2-} (Raman)	---	✓	---	✓	---	×
$v_1PO_4^{3-}$ and $v_3PO_4^{3-}$ (Raman		✓	---	✓	---	×
$v_2PO_4^{3-}$ and $v_4PO_4^{3-}$ (Raman)	---	✓	---	×	---	×
Proline and Hydroxyproline (Raman)	---	✓	---	×	---	×

qRT-PCR and ELISA	**1 Day**	**3 Days**	**7 Days**	**1 Day**	**3 Days**	**7 Days**	**1 Day**	**3 Days**	**7 Days**
Collagen I expression (fold difference)	1.38 ± 0.2	3.7 ± 0.5	0.37 ± 0.2	1.5 ± 0.5	2.7 ± 0.4	1.2 ± 0.3	1.0 ± 0.4	1.8 ± 0.5	0.24 ± 0.1
RUNX 2 expression (fold difference)	2.2 ± 0.4	2.8 ± 0.7	2.7 ± 0.5	2.9 ± 0.4	2.6 ± 0.5	2.4 ± 0.6	1.3 ± 0.3	1.13 ± 0.4	1.0 ± 0.5
Osterix expression (fold difference)	1.4 ± 0.35	2.2 ± 0.33	1.7 ± 0.5	1.04 ± 0.3	2.6 ± 0.5	2.11 ± 0.4	1.0 ± 0.3	0.9 ± 0.2	1.2 ± 0.6
Osteocalcin concentration (ng/ml)	0.34	0.43	1.48	0.35	0.45	1.5	0.33	0.32	0.69